Front. Electr. Electron. Eng. China 2008, 3(3): 353–357
DOI 10.1007/s11460-008-0030-6

RESEARCH ARTICLE

Haifeng SONG, Zhiyu CHEN

# Common-mode radiation characteristic analysis of connections between cables and metal cases



**Abstract** In this paper, the common-mode radiation characteristic of the connection between a cable and a conductor is analyzed by the electric field integral function (EFIF) and the method of moment (MoM). The RWG basis function is adopted as the conductor basis function, the pulse basis function as the wire basis function and the juncture employs Costa basis function. A scheme of singular region separation is proposed to overcome the integration singularity of juncture matrix elements. Some new conclusions of the common-mode radiation characteristics with the metal case are obtained by numeration.

**Keywords** method of moment (MoM), common-mode radiation, metal case, electromagnetic compatibility (EMC)

## 1 Introduction

In the problems of electromagnetic compatibility (EMC), the existence of common-mode radiation has become a significant barrier for various electronic devices that are unable to pass electromagnetic compatibility testing. Common-mode radiation also affects the development of high-frequency and high-speed electronic devices. Therefore, most researchers of EMC pay much attention to decreasing or eliminating the common-mode radiation in the circuits.

Common-mode radiation is caused by the metal case connected by wires. Such structure exists in many electronic devices and communication tools. The problem is commonly encountered when the signal current causes the voltage to drop when impedance exists in the cable or ground return circuit. This voltage drop results in the common-mode radiation. When the cable connects to the metal case, the latter usually becomes a part of the antenna of the common-mode radiation. In consequence, it highly influences the characteristics of the radiation. Currently, a few researches are engaged in such problems and the models used are not common. Furthermore, the introduction of juncture makes it more difficult to deal with the singularity of those matrix units integral. In this paper, we applied the Costa basis function in the juncture region of the line and the surface under Ref. [1]. We also adopted the singular region separateness method of the singularity integrals in the juncture region. This method is suitable for addressing all juncture problems of the line and the surface under any circumstances. Finally, we illustrated a detailed example and made some conclusions that might be useful for practical projects.

Translated from *Chinese Journal of Radio Science*, 2007, 22(3): 375–379 [译自: 电波科学学报]

Haifeng SONG (✉), Zhiyu CHEN
Institute of Electronics, Chinese Academy of Sciences, Beijing 100080, China
E-mail: iecasnico@yahoo.com.cn

Haifeng SONG
China Academy of Electronics and Information Technology, Beijing 100041, China

## 2 Calculation of integral function and selection of basis function

### 2.1 Establishment of calculation model

Figure 1 shows the calculation model. The two metal cases are conductors and connected to the ground. It is assumed that the source of the common-mode radiation is in the middle of the signal back flow line.

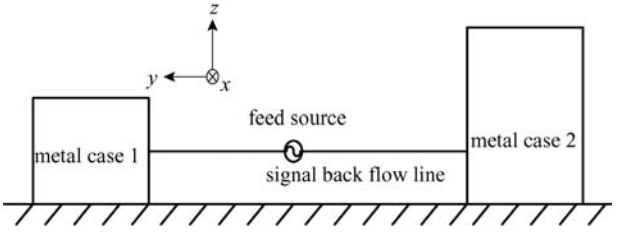


**Fig. 1** Sketch of calculation model

### 2.2 Electric field integral function (EFIF)

Suppose the incidence field is $\boldsymbol{E}^{\text{inc}}(\boldsymbol{r})$, $S$ indicates the surface of the conductor under the irradiation of electromagnetic wave. Generally, $S$ consists of isolated conductors or ones that are connected by wires. Therefore, $S$ should be considered as the combination of all surfaces of conductors and wires. According to the series condition of the tangential electric field on the surface of the conductor ($S$), we can get EFIF

$$\boldsymbol{E}^{\text{inc}}(\boldsymbol{r})_{\tan}=[\mathrm{j}\omega\boldsymbol{A}(\boldsymbol{r})+\nabla\Phi(\boldsymbol{r})]_{\tan},\qquad \boldsymbol{r}\text{ is on }S, \quad (1)$$

where $\boldsymbol{A}$ and $\Phi$ are potential functions:

$$\boldsymbol{A}(\boldsymbol{J},\boldsymbol{r})=\mu\left[\sum_{i=1}^{N_{\text{b}}}\int\int_{S_{B_i}}\boldsymbol{J}(\boldsymbol{r}')G(k,\boldsymbol{r},\boldsymbol{r}')\mathrm{d}s'+\sum_{j=1}^{N_{\text{w}}}\int\int_{S_{W_j}}\frac{I(s')}{2\pi a(s')}\boldsymbol{s}(s')G(k,\boldsymbol{r},\boldsymbol{r}')\mathrm{d}S'\right], \quad (2)$$

$$\Phi(\nabla'\boldsymbol{J},\boldsymbol{r})=-\frac{1}{\mathrm{j}\omega\varepsilon}\left[\sum_{i=1}^{N_{\text{b}}}\int\int_{S_{B_i}}\nabla'_s\boldsymbol{J}(\boldsymbol{r}')G(k,\boldsymbol{r},\boldsymbol{r}')\mathrm{d}s'+\sum_{j=1}^{N_{\text{w}}}\int\int_{S_{W_j}}\frac{1}{2\pi a(s')}\frac{\mathrm{d}I(s')}{\mathrm{d}s'}G(k,\boldsymbol{r},\boldsymbol{r}')\mathrm{d}S'\right], \quad (3)$$

$$G(k,\boldsymbol{r},\boldsymbol{r}')=\frac{\mathrm{e}^{-\mathrm{j}k|\boldsymbol{r}-\boldsymbol{r}'|}}{4\pi|\boldsymbol{r}-\boldsymbol{r}'|}. \quad (4)$$

In Eqs. (2) and (3), $\mathrm{d}S'$ denotes the differential area of $\boldsymbol{r}'$ on the surface ($S_{B_i}$) of the $i$th conductor or the differential area of $s'$ on the surface ($S_{W_j}$) of the $j$th wire. $\boldsymbol{s}(s')$ is the unit vector at the axis of $s'$ of that wire. $N_{\text{b}}$ and $N_{\text{w}}$ denote the number of the conductors and the wires. $a(s')$ is the radius of $s'$ on the $j$th wire.

### 2.3 Decomposition of model and selection of basis function

To approximate the model to the real current distribution and satisfy the continuity of the current in the juncture region, we divided the model into three parts: conductor surface, thin antenna and juncture region. The basis functions applied in the three parts are different.

The conductor basis function: the surface of conductor $i$ employs the triangle part and RWG basis function (as shown in Fig. 2). The corresponding current base function $\boldsymbol{B}_n^i$ [2] against the planar triangle pair with the $n$th border should be

$$\boldsymbol{B}_n^i(\boldsymbol{r})=\begin{cases}\dfrac{l_n^i}{2A_n^{i\pm}}\boldsymbol{\rho}_n^{i\pm}, & \boldsymbol{r}\in T_n^{i\pm},\\ 0, & \text{others},\end{cases} \quad (5)$$

where $\boldsymbol{B}_n^i$ denotes the $n$th basis function of conductor $i$ in the above function.

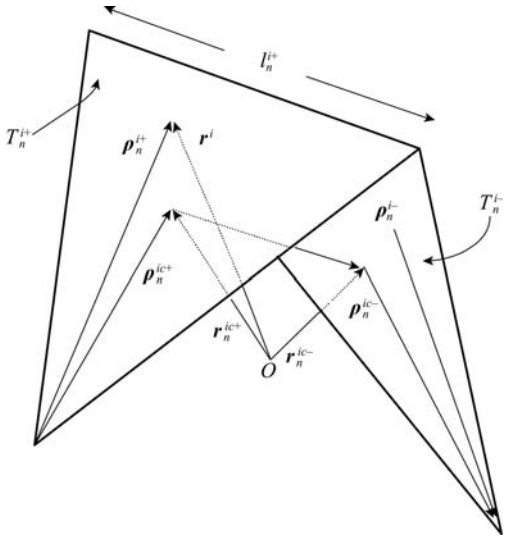


**Fig. 2** RWG basis function

The wire basis function: divide the wire $j$ by proper length and each subsection can be regarded as beeline (as shown in Fig. 3). Therefore, the $n$th basis function $\boldsymbol{W}_n^j$ [3] can be defined as

$$\boldsymbol{W}_n^j(s)=\begin{cases}P_n^j(s)\boldsymbol{s}_{n-1/2}^j, & s_{n-1/2}^j<s<s_n^j,\\ P_n^j(s)\boldsymbol{s}_{n+1/2}^j, & s_n^j<s<s_{n+1/2}^j.\end{cases} \quad (6)$$

In this function, the $P_n^j$ is pulse basis function.

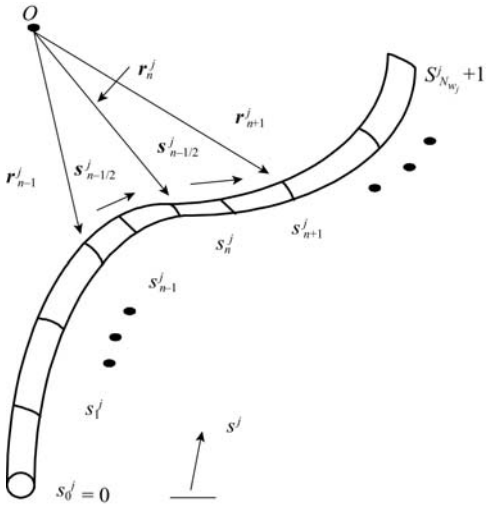


**Fig. 3** Pulse basis function

The basis function of the juncture region: assume that the conductor and the wire have been taken apart by proper triangles and lines, and then the juncture region is the circumjacent area of those junctures. The conductor part of the juncture region is still those triangles which are similar to the conductor surface but the antenna part is the half segment which is connected with the juncture (as shown in Fig. 4). Suppose that the juncture region of wire

$j$ and conductor $i$ is the $k$th juncture region, then its basis function $\boldsymbol{J}^k$ [1] can be defined as

$$\boldsymbol{J}^k(\boldsymbol{r})=\begin{cases}\boldsymbol{f}^k(\boldsymbol{\rho}), & \boldsymbol{r}\text{ is on the conductor part,}\\ \boldsymbol{W}_0^k(s), & \boldsymbol{r}\text{ is on the wire part,}\\ 0, & \text{others.}\end{cases} \quad (7)$$

In this function, $\boldsymbol{W}_0^k(s)$ can be expressed as $\boldsymbol{W}_0^k(s)=p_0^k(s)\boldsymbol{s}_{1/2}^k$, and $\boldsymbol{f}^k(\boldsymbol{\rho})$ in triangle $T_n^k$ can be expressed as

$$\boldsymbol{f}^k(\boldsymbol{\rho})=\boldsymbol{f}_n^k(\boldsymbol{\rho}_n)=-\frac{1}{\alpha_t^k}\frac{[1-(1-\eta)^2]}{\rho_n^2}\boldsymbol{\rho}_n,\quad \boldsymbol{r}\text{ is inside }T_n^k, \quad (8)$$

where $\boldsymbol{\rho}_n=\boldsymbol{r}-\boldsymbol{r}_0$, $\boldsymbol{r}$ is the coordinate of the arbitrary point inside the triangle and $\boldsymbol{r}_0$ is the coordinate of the juncture. For certain triangle $T_n^k$ in the juncture region, if the vertex denotes the juncture, then $\boldsymbol{r}_0=\boldsymbol{r}_p$, $\eta=A_p/A_n^k$, $A_p$ ($p=1, 2, 3$) depicts the area of the triangle which is composed of point $p$ and the remaining two vertexes, $A_n^k$ is the whole area of the triangle $T_n^k$, $N_{J_k}$ are the numbers of the triangles included in the juncture region $k$ where wire $j$ exists. $\alpha_t^k$ is the sum of all angles related with juncture points in juncture region $k$.

The processing of singularity integrals: the following singular integrals need to be processed:

$$I_1=\iint_{T_n}\frac{\mathrm{e}^{-\mathrm{j}kR}}{R}\mathrm{d}s',\ I_2=\iint_{T_n}\frac{\mathrm{e}^{-\mathrm{j}kR}}{R}\boldsymbol{\rho}_n\mathrm{d}s',\ I_3=\int_S\frac{\mathrm{e}^{-\mathrm{j}kR_a}}{R_a}\mathrm{d}s',$$

$$I_4=\iint_{T_n^k}\boldsymbol{f}_n^k(\boldsymbol{\rho}')\cdot\frac{\mathrm{e}^{-\mathrm{j}kR}}{R}\mathrm{d}s',\ I_5=\iint_{T_n^k}\nabla_s'\cdot\boldsymbol{f}_n^k(\boldsymbol{\rho}')\frac{\mathrm{e}^{-\mathrm{j}kR}}{R}\mathrm{d}s'.$$

Refer to Ref. [2] for the processing of $I_1$ and $I_2$ and Ref. [3] for that of $I_3$, respectively. The singularity region separateness method is applied when processing $I_4$ and $I_5$. The detailed method is as follows:

Putting Eq. (8) into $I_4$, we can obtain the flowing integral:

$$I_4'=\iint_{T_n^k}\frac{\left[1-(1-\eta)^2\right]\boldsymbol{\rho}_n}{\rho_n^2}\cdot\frac{\mathrm{e}^{-\mathrm{j}kR}}{R}\mathrm{d}s',$$

$$\boldsymbol{\rho}_n=\boldsymbol{r}'-\boldsymbol{r}_0,\quad \rho_n=|\boldsymbol{r}_0-\boldsymbol{r}'|,\quad R=|\boldsymbol{r}_c-\boldsymbol{r}'|.$$

As is illustrated in Fig. 4, $\boldsymbol{r}_0$ denotes the juncture, $\boldsymbol{r}_c$ the center point of the singularity triangle, $\boldsymbol{r}'$ the source point. Obviously, $\boldsymbol{r}_0$ and $\boldsymbol{r}_c$ are two singularity points. Now we establish a sub-triangle with the center point of the original triangle. We can attain the sub-triangle 7 as shown in Fig. 5. For simplicity, the sub-triangles are chosen as the original triangle to form the similar triangle, and then by connecting all vertexes of both the original and sub triangles, we can obtain 7 triangles—1, 2, 3, 4, 5, 6 and 7 as shown in Fig. 5. Noticeably, the integral of $I_4'$ does not exhibit a singularity point inside the sub-triangles 4, 5 and 6. Since the singularity point $\boldsymbol{r}_0$ inside triangles 1, 2 and 3 rest on the vertex, it has a very similar effect if we apply the 7 point Gauss integral [4–7], which does not cross the singularity point. Therefore, no special process is demanded. The center point $\boldsymbol{r}_c$ is the singularity point inside the sub-triangle 7. By calculation, we can obtain the function

$$I_{4(7)}'=-\mathrm{j}k\iint_{T_{n(7)}^k}\frac{\left[1-(1-\eta)^2\right]\boldsymbol{\rho}_n}{|\boldsymbol{r}_0-\boldsymbol{r}'|^2}\mathrm{d}s'+\frac{\left[1-(1-\eta)^2\right]}{|\boldsymbol{r}_0-\boldsymbol{r}_c|^2}\left(\iint_{T_{n(7)}^k}\frac{\boldsymbol{r}'-\boldsymbol{r}_c}{|\boldsymbol{r}_c-\boldsymbol{r}'|}\mathrm{d}s'+(\boldsymbol{r}_c-\boldsymbol{r}_0)\iint_{T_{n(7)}^k}\frac{1}{|\boldsymbol{r}_c-\boldsymbol{r}'|}\mathrm{d}s'\right).$$

Likewise, the processing of the singularity integral of $I_5$ can be dealt with in a similar way.

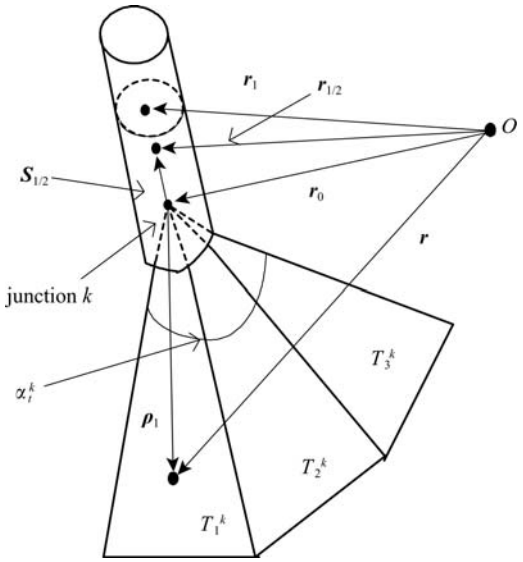


**Fig. 4** Costa basis function

## 3 Experiment validation

To investigate the validity of the method, the calculated results are tested by experiment. The experiment model is illustrated in Fig. 1. There is a 10 μH inductor at the middle of the signal back flow line. A 100 mV voltage signal from the signal source Marconi 2022C (metal case 2) produces difference-mode current through inductance $L$ and 50 Ω load (metal case 1), and generates common-mode voltage, namely feed source at the place of the inductance. The length, width and height of the metal case 1 are 20, 10 and 5 cm, respectively, and for metal case 2 the corresponding size is 20, 33 and 13 cm. The length of the signal back flow line is 1 m and it is 2.5 cm from the ground. The experiment was conducted in a darkroom of 1 m EMC.

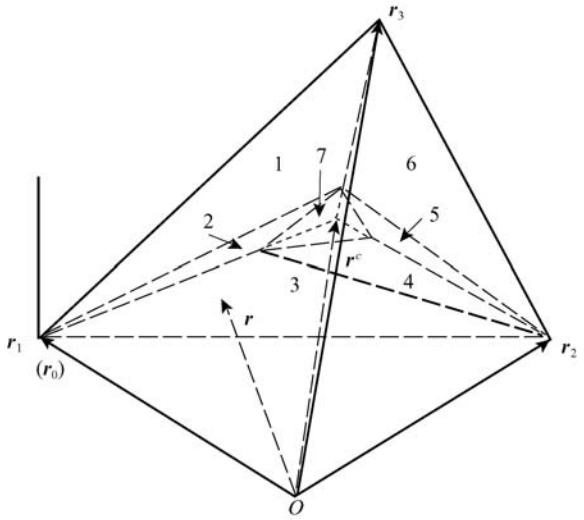


**Fig. 5** Singular region separateness

The double cones antenna, ZN 30504A are placed in a horizontal level and 52 cm away from the ground. We can see from Fig. 6 that the result gained by the method applied in our paper is close to the experimental data.

## 4 Common-mode radiation characteristics analysis

Based on the above calculation, we conclude the characteristics of common-mode radiation when the metal case exists.

### 4.1 Distribution characteristics of electric field and magnetic field

Figure 7 is the distribution chart of the electric field and magnetic field while setting the example at 100 MHz. The

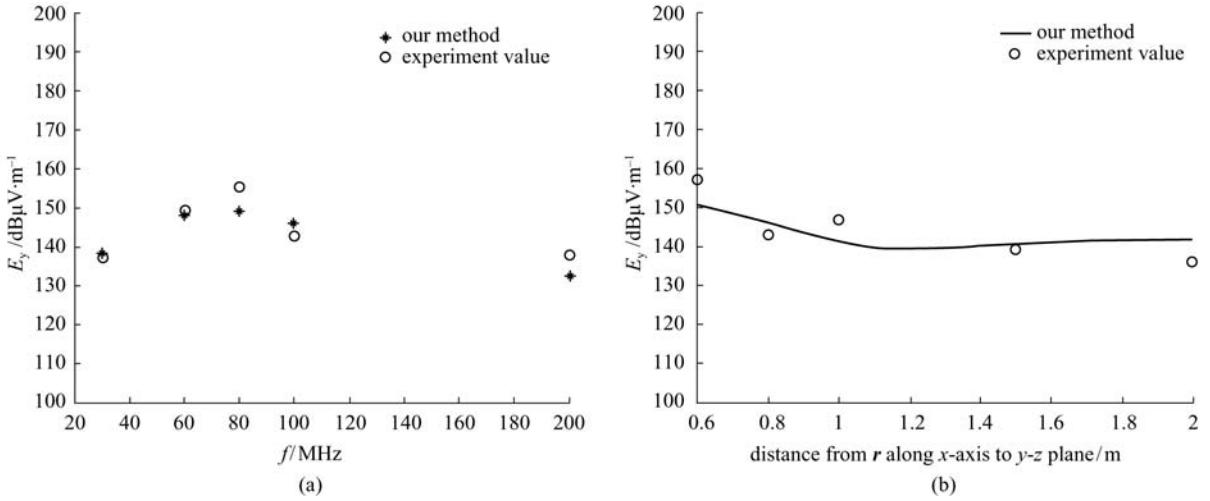


**Fig. 6** Comparison of theoretical value and experiment value of $E_y$. (a) $E_y$ on some frequency points when $r = 0.8$ m; (b) $E_y$ on some distance points when $f = 100$ MHz

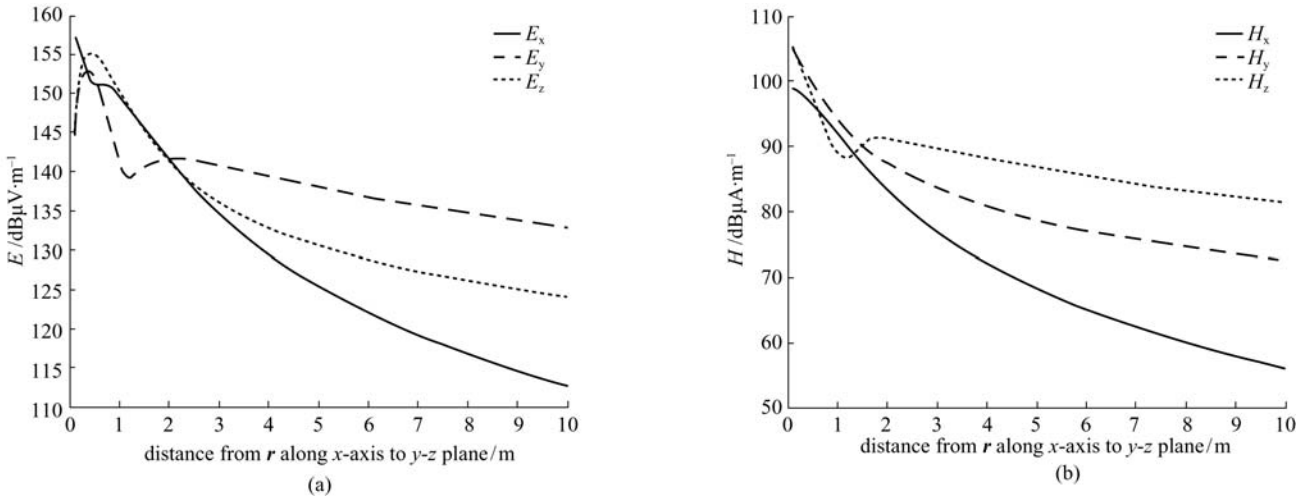


**Fig. 7** Distribution of electric field and magnetic field under calculation model. (a) $E$; (b) $H$

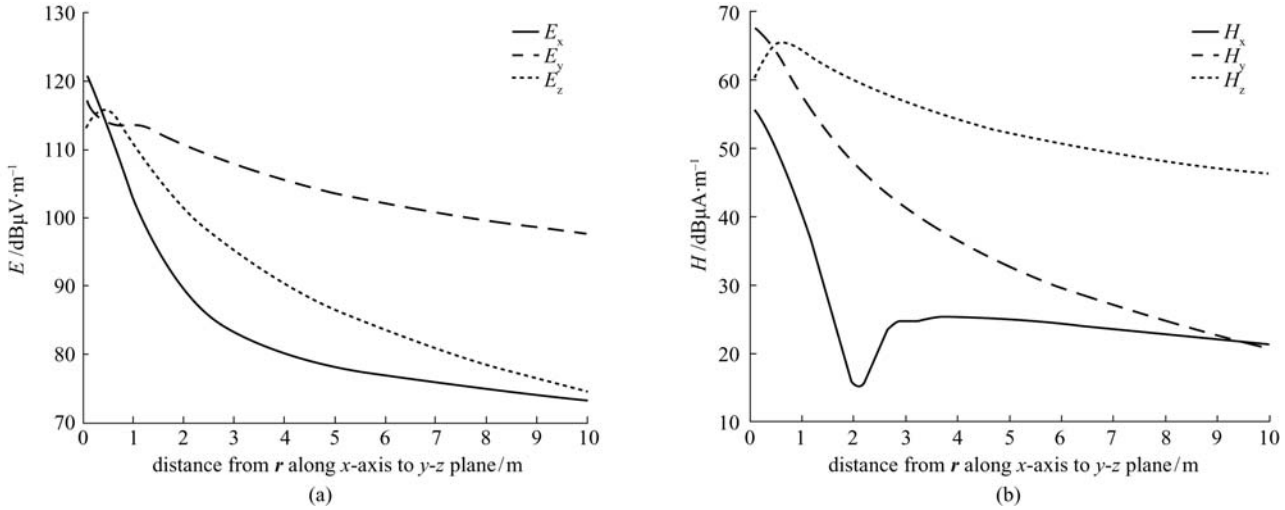


**Fig. 8** Distribution of electric field and magnetic field under model with smaller metal case. (a) $E$; (b) $H$

chart shows that the electric field and the magnetic field are mainly focused on $E_y$ and $H_z$ respectively in the far field region. Furthermore, the calculated wave impedance is about 376 Ω in the far field region and meets the characteristics of the plane wave therein. However, the relationship among each component is complicated in the near-field region.

### 4.2 Impact of size of metal case to radiation field

Keeping the same model, we assume that the two metal cases have the same size. The length, width and height of both cases are 2 cm, 2 cm and 5 cm, respectively, thus diminishing both sizes of the two metal cases. The calculated radiation fields are shown in Fig. 8. The chart shows that when the cases are getting smaller the radiation field is getting smaller, and the ratio of $E_y$ and $H_z$ compared with other corresponding components is getting larger.

### 4.3 Relationship with frequency $f$

A few frequency points are calculated by applying our method and the conclusion is that: in the far field region, $E_y$ is dominant in the electric field and $H_z$ is dominant in the magnetic field. Furthermore, the higher the frequency is, the clearer is this trend. However, the change of the radiation intensity and the change of frequency are not in direct proportion, which is illustrated in Fig. 6(a).

## 5 Conclusions

With the rapid development of electronics technology, more and more communications devices are being produced. Therefore, the problems of EMC are attracting much more attention. In this paper, the characteristics of common-mode radiation between two metal cases connected with wires are investigated by the method of EFIF combined with method of moment (MoM). The Costa basis function in the juncture region and the singularity region separation method for the singularity integrals are adopted. This method applies to the connecting circumstances under arbitrary line antenna and arbitrary conductor. Compared with the experimentation, the calculation result is credible. Some characteristics of common-mode radiation with metal case are educed, which can be referred to by engineers in the field of EMC.

## References

1. Rao S M, Wilton D R, Glisson A W. Electromagnetic scattering by surfaces of arbitrary shape. IEEE Transactions on Antennas and Propagation, 1982, 30(3): 409–418
2. Wilton D R, Rao S M, Glisson A W. Potential integrals for uniform and linear source distributions on polygonal and polyhedral domains. IEEE Transactions on Antennas and Propagation, 1984, 32(3): 276–281
3. Harrington R F. Field Computation by Moment Methods (in Chinese, trans. Wang Erjie and Xiao Liangyong). Beijing: National Defense Industry Press, 1981: 73–141
4. Jin Jianming. The Finite Element Method in Electromagnetics. (in Chinese, trans. Wang Jianguo). Xi'an: Xidian University Press, 1998
5. Costa M F, Harrington R F. Minimization of radiation from computer systems. In: Proceedings of International Electronics Conference and Exposition, 1983, (9): 660–665
6. Costa M F. Electromagnetic radiation and scattering from a system of conducting bodies interconnected by wires. Dissertation for the Doctoral Degree. Syracuse University, 1983
7. Li Shizhi. The MoM Applied in the Problems of Electromagnetism Fields. Beijing: Publishing House of Electronics Industry, 1985 (in Chinese)